ISSN 1070-4272, Russian Journal of Applied Chemistry, 2015, Vol. 88, No. 5, pp. 846−851. © Pleiades Publishing, Ltd., 2015.
Original Russian Text © S.R. Egorova, A.N. Mukhamed'yarova, A.A. Lamberov 2015, published in Zhurnal Prikladnoi Khimii, 2015, Vol. 88, No. 5, pp. 805−811.

VARIOUS TECHNOLOGIES

Specific Features of the Phase Transition of Gibbsite into Boehmite under Hydrothermal Treatment of Floccules in an Aqueous Suspension

S. R. Egorova, A. N. Mukhamed'yarova, and A. A. Lamberov

Kazan (Volga Region) Federal University, ul. Kremlevskaya 18, Kazan, Tatarstan, 420000 Russia
e-mail: segorova@rambler.ru

Received March 20, 2015

Abstract—Effect of the conditions in which floccules of gibbsite are hydrothermally treated on the phase composition of products of its dehydration products, obtained at T = 180–210°C and P = 1.0–1.9 MPa was studied. The phase transition of gibbsite into boehmite occurs by the dissolution–deposition mechanism upon delamination of gibbsite crystals along the (001) plane to give a multitude of layers with thicknesses of 20–100 nm and cracks in between, with widths of 10–50 nm. In the dissolution of gibbsite, $[Al(OH)_4]^-$ anions pass into solution and react with protons of hydroxy groups on the (001) planes of gibbsite, with the subsequent nucleation of boehmite and growth of its crystals. The crystallization of coarse boehmite particles favors formation of nonporous floccules. Boehmite particles form no strong crystallization bonds with each other, which impairs their abrasion resistance.

DOI: 10.1134/S1070427215050195

An important place in catalytic processes of the petrochemical synthesis, such as dehydrogenation of lower paraffins and oxidative chlorination of ethylene, performed in a fluidized bed, is occupied by microspherical catalysts produced on aluminum oxide supports with a γ-Al2O3 structure, which a large surface area and grains with sizes of 20–250 μm [1, 2]. The precursor phase of γ-Al_2O_3 is boehmite (Bm) or pseudoboehmite, which can be produced in various ways by processing of coarse gibbsite (Gb) floccules. For example, dehydration of gibbsite under atmospheric pressure in severe conditions ($T \approx 350$°C) yields a boehmite concentration not exceeding 56 wt % in floccules [3]. In contrast to the thermal treatment of gibbsite, that under hydrothermal conditions favors a complete phase transition to boehmite even at $T > 150$°C and at a higher rate [4]. One of variants is the hydrothermal treatment (HTT) of floccules in a closed volume in the "dry steam" medium at T = 200°C and P = 17 kg cm^{-2}, when the elevated pressure is created in a vessel only by the water vapor released in dehydration of gibbsite. In this case, however, the gibbsite–boehmite phase transition is accompanied by full dispersion of floccules into a placer of needle-like boehmite particles with sizes of 2 to 20 μm [5].

At present, there is no unambiguous opinion about the mechanism of gibbsite recrystallization into boehmite under hydrothermal conditions. According to the opinion of several authors [6–8], the solid-phase mechanism of gibbsite conversion to boehmite is operative in the "dry steam" medium at small amounts of released water. In an aqueous suspension or in lower alcohols, the dissolution–precipitation mechanism is possible, with a more pronounced mass transfer of complex-forming components across the liquid phase to the surface of aluminum oxide or hydroxide particles subjected to recrystallization [4, 9, 10]. For example, processes of boehmite crystallization of gibbsite particles with average size of 0.2 to 100 μm in the temperature range 160–350°C at the corresponding pressures of the saturated water vapor have been described [4, 7–15]. In [8], a direct relationship was revealed between the crystallization rate and the size of precursor particles.

The conditions of the HTT of gibbsite, reported in various communications, noticeably vary. For this

reason, there is no unambiguous opinion about the time required for a complete phase transition into boehmite. For example, boehmite was obtained in [15] at 180 and 190°C only in 120 and 50 h, respectively; it was found in [4, 10] that, at 200 and 220°C, boehmite crystallizes in 1–2 and approximately 0.5 h, respectively. In a number of studies, dispersion of starting phase particles was also noted. According to [13], the particle size becomes nearly 50 times smaller in HTT. Data on the size of coherent scattering regions (CSRs) of boehmite crystals being formed, type of crystal packing, and effect of these on the porous system parameters of HTT products have not been reported in the literature, either. The reason is that studies of the gibbsite–boehmite phase transition are predominantly aimed to find how the HTT conditions affect the crystallization of corundum in milder modes, compared with the atmospheric thermal treatment.

To determine whether a microspherical boehmite support can be formed for dehydrogenation catalysts and to optimize the formation conditions, we examined in the present study the influence exerted by the conditions of HTT of coarse, 40–180 μm in size, gibbsite floccules on the kinetics of the phase transition to boehmite, their porous system, morphology of boehmite particles, and their physicomechanical characteristics in the temperature range 180–210°C in an aqueous suspension (pH 6.0–10.5) at an appropriate saturated vapor pressure of water.

EXPERIMENTAL

As the starting compound served gibbsite of GD00 brand (Bogoslovskii aluminum plant OAO). Floccules 40–180 μm in size were selected for studying the phase transition.

The HTT of the floccules was performed in a Вьchiglasuster Limbo li autoclave with automated temperature and pressure control in a 450-mL stainless steel reactor at an aluminum hydroxide mass ratio of 1 : 5 under agitation with a stirrer at a speed of 500 rpm and maximum degree of autoclave filling of 70%. The pH value of the starting aqueous suspension of gibbsite was 10.5. The medium was alkalized via passing of a part of sodium ions from gibbsite floccules into solution. The pH values of 8.0 and 6.0 were provided by addition of an acetic acid solution to the suspension. In kinetic studies, the instant when a prescribed reaction temperature was reached in the autoclave reactor was taken as the starting point. The prescribed temperature was reached in approximately 60 min. The autoclave reactor was cooled by feeding cold water into its jacket. As a result, its temperature decreased by 100° during 20 min.

An X-ray phase analysis was made on a Shimadzu XRD-7000 diffractometer with long-wavelength CuK_α radiation and a graphite monochromator. The range of 2θ angles was 5–90° with a step of 0.05°. The phase identification was carried out in accordance with the presence in the spectrum of the following diffraction lines: γ-$Al(OH)_3$ (ICSD 200599), γ-AlOOH (ICSD 6162), γ-Al_2O_3 (ICSD 66559), χ-Al_2O_3 (ICSD 13-373). The CSR sizes were calculated by the Selyakov–Scherrer formula. The error in determining the CSR size was about 10%.

A thermal analysis[1] (TA) was made on a Netzsch STA-449C Jupiter combined TG-DSC analyzer coupled with a QMS 403 Aeolos quadrupole mass spectrometer in the temperature range 30–1000°C at a heating rate of 10 deg min^{-1} in a flow of argon. The phase concentrations were calculated from the amount of water released in dehydration of aluminum hydroxides with consideration for the fact that boehmite and χ-Al_2O_3 phases are formed in an approximately 1 : 1 mass ratio in thermal decomposition of gibbsite.

The specific surface area S and pore volume V were measured on a Quantachrome Autosorb iQ versatile analyzer. The specific surface area was calculated on the basis of the surface area of the nitrogen molecule of 0.162 nm^2 and N2 density in the standard liquid state of 0.808 g cm^{-3}. The measurement accuracy was 0.1 $m^2 g^{-1}$ ± 5%. Adsorption isotherms were obtained at –196°C upon degassing of a sample at 500°C to a residual pressure of 0.013 Pa. The distributions of pore volumes over pore diameters were calculated from the desorption branch of the isotherm by using the standard Barrett–Joyner–Highland procedure [16]. The measurement accuracy was ± 5%.

IR spectroscopic measurements were made on a Bruker VERTEX 70 instrument at room temperature. Samples were compacted into pellets with KBr. Spectra were recorded with a resolution of 1 cm^{-1} and averaged over 128 scans.

Studies by scanning electron microscopy (SEM) were carried out on an EVO 50 XVP electron microscope combined with an INCA 350 energy-dispersive spectrometer. The resolution of the spectrometer was 130 eV. The analysis was made at an accelerating voltage of 20 kV at a path length of 8 mm.

The floccule size distribution was analyzed in conformity with the ASTM B821-10 standard on a

Table 1. Effect of gibbsite HTT conditions on the CSR size of gibbsite and boehmite crystals

HTT conditions				CSR sizes, nm			
				gibbsite		boehmite	
T, °C	*P*, MPa	τ, min	pH	$D_{(002)}$	$D_{(110)}$	$D_{(020)}$	$D_{(120)}$
Starting gibbsite				67.5	55.0	–	–
180	1.0	150	10.5	75.9	70.7	60.5	35.9
		240		76.1	71.8	61.3	36.4
		30		72.5	70.3	60.9	–
190	1.3	60	10.5	74.8	72,4	62.7	36.6
		240		–	–	74.2	55.3
190	1.3	60	8.0	71.2	74.9	61.0	–
		90		79.7	81.8	71.0	51.5
		120		100.1	83.0	67.4	51.5
		150		104.0	86.5	71.8	53.3
190	1.3	120	6.0	102.8	85.4	76.2	54.2
		150		106.2	83.8	80.4	59.7
		240		–	–	79.5	50.7
200	1.6	20	10.5	71.4	72.5	62.8	–
		30		102.5	88.8	81.1	55.3
		90		–	–	82.7	54.7
		240		–	–	79.8	59.6
210	1.9	0	10.5	100.1	85.1	74.2	47.0
		20		–	–	64,0	55.2
		240		–	–	66.7	51.1

[a] Data of [9] are reported for comparing.

[b] Compositions were filled with silanized fine dispersed quartz powder in an amount of 77 wt %.

Malvern Mastersizer 2000 laser diffraction analyzer equipped with a Hydro 2000S wet sample dispersion unit.

The abrasion resistance of floccules was found from their wear in a fluidized bed during 1 h in a quartz tube with height of 100 cm and diameter of 32 mm in a jet of air delivered through a nozzle with diameter of 0.4 mm at a flow rate of 320 L h^{-1}, situated in the lower part of the tube. After the test, the mass of <0.4-μm particles carried away from the tube was measured.

^{27}Al NMR spectra were recorded with an Avance II 500 spectrometer at a frequency of 130.32 MHz. The samples had the form of a mixture of solutions under study in an amount of 550 μL with addition of 50 μL of D_2O. The spectra were recorded twice, from only samples under study and with a capillary filled with an ammonium chloride solution additionally placed in the ampule. The concentration of AlCl3 was 0.2 M. The capillary had inner and outer diameters of 0.8 and 1.35 mm, respectively. The inner diameter of the ampules was 4.2 mm. The temperature was 25°C. The 27Al NMR spectra were recorded with rectangular (broadband) pulses with width of 8 μs and power of 80 W (rotation angle <90°); the relaxation delay was 1 s. The number of accumulations was 400–800, and the width of the spectrum, 504.8 ppm. The spectra were processes by digital exponential filtration

with a constant LB = 3 Hz. The error in determining the chemical shift was ±0.05 ppm.

RESULTS AND DISCUSSION

The phase composition of the products of gibbsite dehydration was determined from the set of XPA and TA data. It follows from an analysis of the X-ray diffraction patterns of samples obtained upon HTT of gibbsite that boehmite is the final product in all cases. No diffraction lines corresponding to other oxo hydroxide compounds of aluminum appear. Effects due to the dehydration of unconverted gibbsite and boehmite being formed are identified in DTG–DSC curves of the samples. In the DSC curves, the endothermic effects of gibbsite dehydration to boehmite and χ-Al_2O_3 appear as minima in narrow temperature ranges 257–260 and 315–352°C, and that of boehmite to γ-Al_2O_3, in the range from 539 to 561°C, irrespective of the treatment temperature. With the HTT duration increasing to 240 min, the loss of mass in this range of the boehmite dehydration effect grows from 4.5 to 14.5–15.0 wt %, which is indicative of the complete phase transition of gibbsite into boehmite. As the HTT temperature is raised, the endothermic minimum is shifted to larger values by approximately 20°, which evidences that, under the prescribed conditions, the size of primary boehmite crystals grows only slightly with its increasing fraction in the samples.

The results of the thermal analysis are confirmed by calculations of the CSR size incrystals of boehmite being formed, which vary from 60.5 to 82.7 nm and from 35.9 to 59.7 nm along the (020) and (120) planes, respectively (Table 1). For example, at a boehmite content of up to 25 wt %, the CSR sizes in the (020) plane are 60.5–62.7 nm, and those in the (120) plane, 35.9–36.6 nm. These sizes further, upon the complete phase transition of gibbsite into boehmite, grow (Fg. 1). In this case, the crystallization processes and the tendency toward the subsequent increase in the CSR sizes of boehmite are identical for the planes under consideration for all the chosen HTT temperatures and pH values of the aqueous suspension. The dependences of the CSR size on the concentration of boehmite in floccules are step-like for both planes. Here, as follows from the data in Table 1, the CSR sizes of boehmite crystals in the samples are correlated with the averaged CSR sizes in crystals of residual gibbsite, which are 67.5 and 55.0 nm for the (002) and (110) planes, respectively.

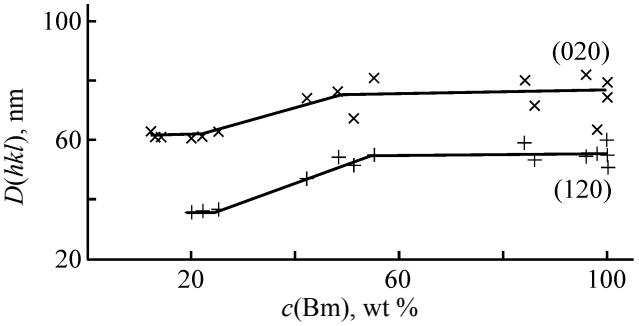

Fig. 1. CSR sizes $D(hkl)$ of boehmite crystals vs. the boehmite concentration c(BM) in products formed in the HTT of gibbsite.

Consequently, coarse primary particles of boehmite are already formed in the initial stages of the phase transition of gibbsite under the hydrothermal conditions. For example, even at low concentrations (up to 30.0 wt %) of boehmite in samples produced by HTT at temperatures of 180, 190 ($\tau \leq 60$ min), and 200°C ($\tau \leq 20$ min), at which the diffraction lines characteristic of boehmite can be distinguished in X-ray diffraction patterns of mixtures with gibbsite, the CSR size for crystals of the phase being formed are very close to those for the precursor crystals. In this case, the CSR sizes of crystals of the remaining gibbsite grow, due to the transformation of smaller size particles, to 72.5–76.1 nm along the (002) plane and to 70.3–74.9 nm along the (110) plane. With increasing fraction of converted gibbsite and growing boehmite content, the SCR sizes of residual gibbsite reach values of 106.2 nm along the (002) plane and 88.8 nm along the (110) plane. Thus, it can be assumed that, first, gibbsite particles with smaller CSR undergo a phase transition at low temperature (T = 180°C) and long HTT duration (150–240 min) or at high temperature (T = 190–200°C) and short HTT duration (20–90 min), for which comparatively low (1.0–1.6 MPa) water vapor pressures are sufficient, and then this occurs with particle having larger CSRs, which are recrystallized into boehmite at higher water vapor pressures (1.6–1.9 MPa).

Probably, it is the presence of particles with various size that is responsible for the partial phase transition of gibbsite into boehmite at 180°C, which does not exceed 22.0 wt %, and also for the step-like run of the kinetic curves describing the formation of boehmite (Fig. 2). For example, the curves are of the sigmoid type in the range 180–200°C, but are transformed into a leveling-off curve at 210°C, when the corresponding saturated

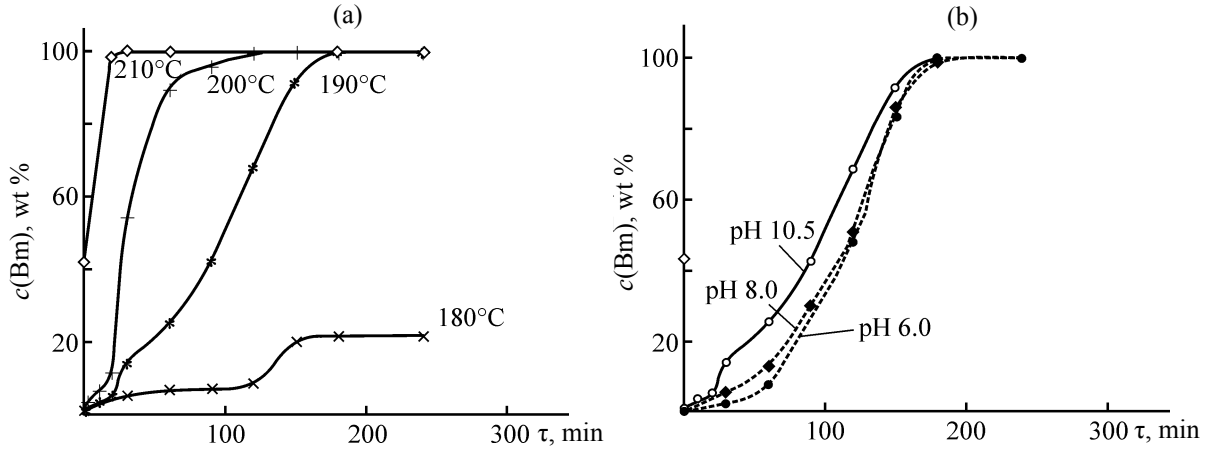

Fig. 2. Kinetic curves of boehmite formation in the HT orthoferrite at (a) pH 10.5 and (b) 190°C. [*c*(Bm)] Content of boehmite and (τ) time.

vapor pressure of water is sufficient for an accelerated transformation of gibbsite particles with all CSR sizes.

It follows from the data in Table 2 that, with the temperature increasing from 180 to 210°C (pH 10.5), the rate constant of boehmite formation grows by more than a factor of 20. The kinetic curves of boehmite formation are described with the highest reliability (R^2 = 0.8958–0.9902) by the Avrami–Erofeev–Kolmogorov equation. The exponent n = 3 in the equation indicates that there grow 3D nuclei of boehmite [17], which is confirmed by the SEM method (Fig. 3). It can be seen in the images of the samples that aggregates of boehmite crystals in the bulk of floccules acquire the shape of rhombs and parallelepipeds. In this case, the sizes of primary crystals visually identified in the images with the maximum magnification (Fig. 3) are close to the CSR sizes along the (020) plane.

The apparent activation energy of the process is 172 ± 7 kJ mol^{-1}, in agreement with the known published data [4]. The value obtained is 2.7 times that in the case of the atmospheric thermal treatment of gibbsite [3]. The reason is that the phase transition of gibbsite into boehmite occurs under hydrothermal conditions with a noticeable induction period, which is 120 min at 180°C, but diminishes to 20–30 min at 190–200°C. At 210°C, no induction period is observed at all (Fig. 2). The induction period is affected by the suspension pH: it becomes noticeably longer as the pH value decreases from 10.5 to 6.0–8.0. For example, the induction period increases from 60 to 60 min at 190°C. As follows from the data in Table 2, reducing the pH value of the suspension from 10.5 to 6.0 also makes the crystallization rate constant of boehmite 1.5 times lower. This occurs because gibbsite is partly dissolved during this interval of time and aluminum ions are released into the aqueous solution and are further involved in the crystallization of the boehmite phase.

The dissolution is confirmed by the results of a ^{27}Al NMR analyses of mother liquors of the suspension of aluminum hydroxides, isolated upon the HTT of gibbsite (Fig. 4). For example, the ^{27}Al NMR spectra of solutions obtained at 200 and 210°C during 30–60 min

Table 2. Kinetic characteristics of the reaction by which boehmite is formed in HTT of gibbsite (Avrami–Erofeev–Kolmogorov function)

T, °C	pH	k, s^{-1}	n	R^2	E_a, kJ mol^{-1}
180	10.5	4.0×10^{-5}	4.0	0.8958	172 ± 7
190		1.5×10^{-4}	3.0	0.9275	
200		2.2×10^{-4}	3.0	0.9622	
210		8.3×10^{-4}	3.0	0.9902	
190	8.0	1.2×10^{-4}	3.0	0.9655	
	6.0	1.0×10^{-4}	3.0	0.8994	

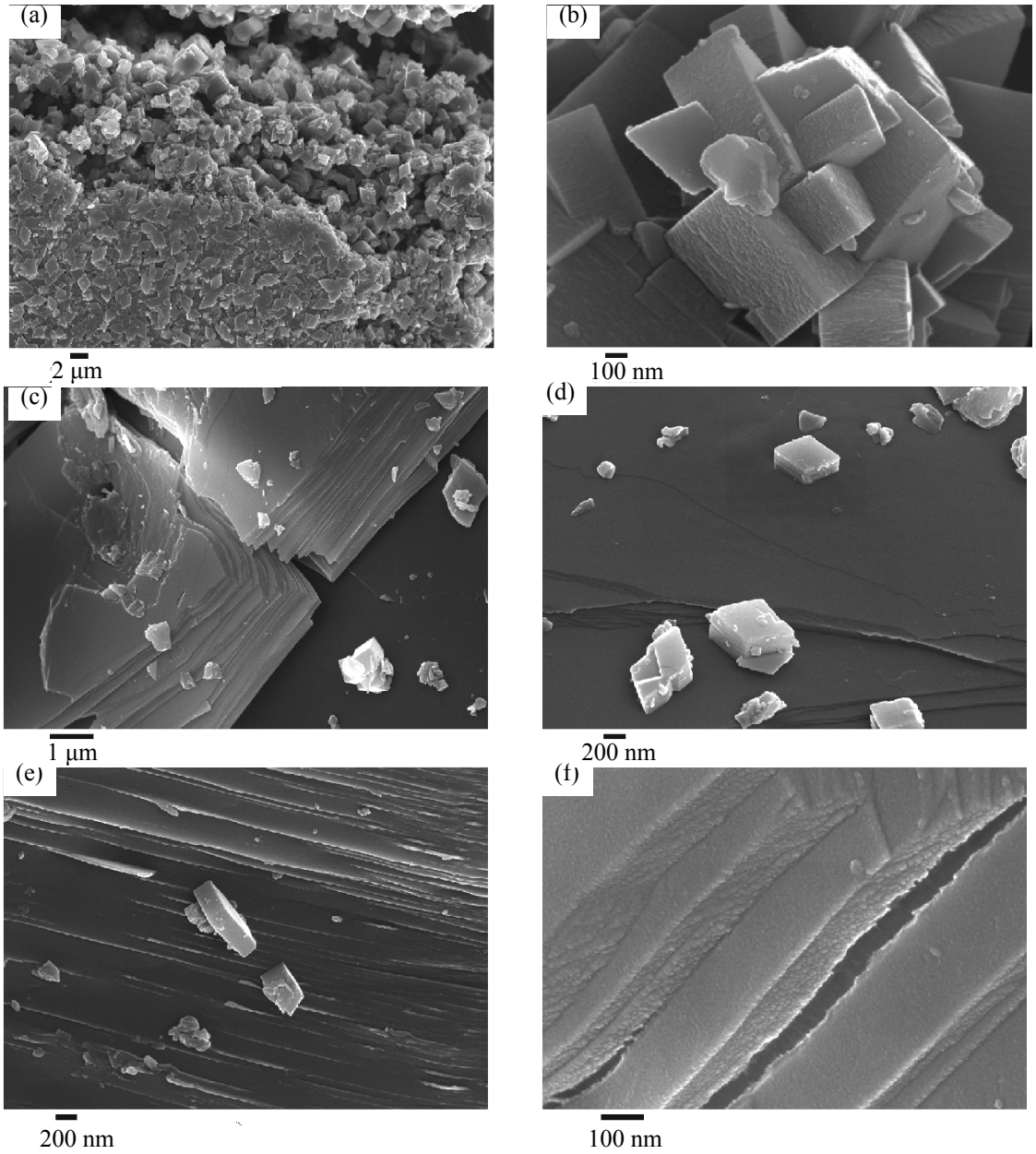

Fig. 3. SEM images gibbsite HTT products obtained at (a, b) T = 200°C, τ = 120 min, and pH 10.5 and (c, d) T = 180°C, τ = 180 min, and pH 10.5. (a) Cross-section of a floccule, (b) aggregates of boehmite crystals, (c) gibbsite crystals upon delamination, (d, e) boehmite crystals on planes of gibbsite crystals, and (f) layers of gibbsite crystals and slits in between.

at various pH values contain, in addition to the signal with a chemical shift of 0.7 ppm, which corresponds to aluminum cations in the complexes $[Al(H_2O)_6]^{3+}$ in an aqueous solution of $AlCl_3$, used as an external standard, the signal with a chemical shift of 80.7 ppm. This signal is due to the presence in solution of mononuclear anions $[Al(OH)_4]^-$, known [18, 19] to be formed via dissolution of aluminum hydroxides. The intensity of the signal of aluminum atoms in $[Al(H_2O)_6]^{3+}$ complexes in the standard $AlCl_3$ solution with the concentration of aluminum atoms set to 0.2 M is taken as 100%.

According to the results of integration and recalculation, the concentrations of aluminum atoms in the mother liquors under study were in the range from 0.01 to 1.06 M (Table 3). With the HTT duration increasing from 30 to 60 min, the concentration of aluminum atoms in solution grows and, accordingly, so does the amount of $[Al(OH)_4]^-$ anions, which indicates that the fraction of dissolved

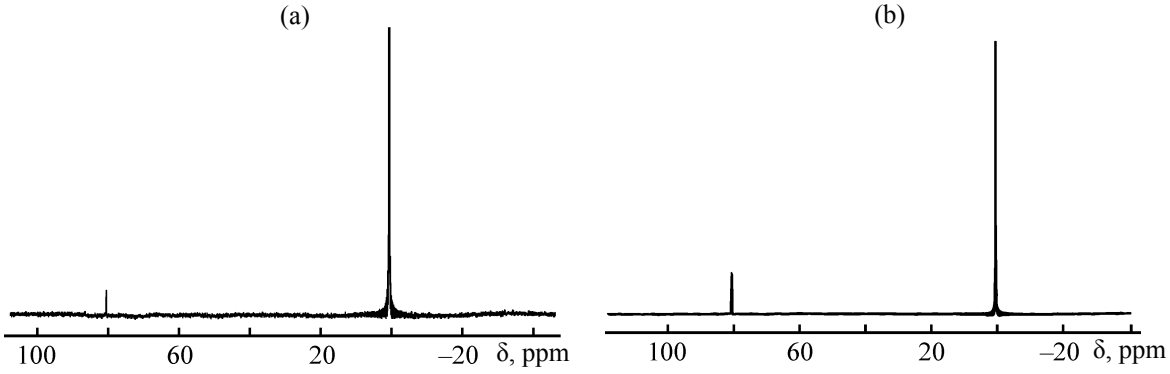

Fig. 4. ^{27}Al NMR spectra of samples of other liquors of a suspension of aluminum hydroxides isolated upon HTT of gibbsite at 200°C and pH 10.5 during (a) 30 and (b) 60 min with a standard AlCl3 solution. (δ) Chemical shift.

aluminum hydroxide becomes larger. Mostly gibbsite is dissolved under the specified conditions, which follows from the dependence shown in Fig. 5. It can be seen that, as the complete phase transition of gibbsite into boehmite is approached, the concentration of aluminum atoms in the mother liquor changes only slightly. At the same time, the dependence of the boehmite content on the concentration of aluminum atoms in solution by itself takes the form of a leveling-off curve.

The signals of $[Al(OH)_4]^-$ anions are also identified in ^{27}Al NMR spectra of mother liquors with pH 10.5, obtained on boiling an aqueous suspension of gibbsite under atmospheric pressure for 60 and 180 min. The concentrations of aluminum in the solutions are 0.13 and 0.29 mM, respectively. Consequently, the process in which gibbsite is dissolved and $[Al(OH)_4]^-$ anions are formed is intensified under the HTT conditions.

The crystallization of boehmite is possible via interaction of the anions with protons of hydroxy groups on planes of gibbsite crystals by the scheme

$$[Al(OH)_4]^- + H^+ \rightarrow AlO(OH) + 2H_2O.$$

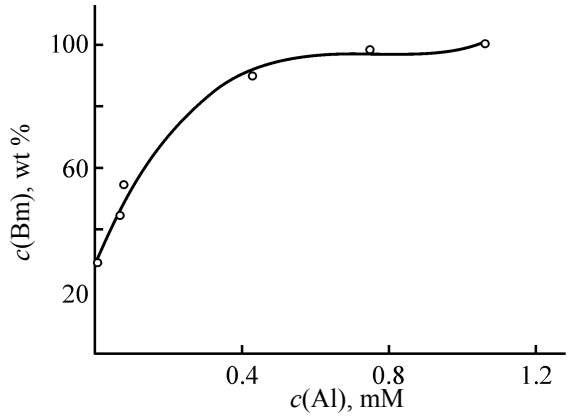

Fig. 5. Concentration c(Al) of aluminum atoms in the mother liquor vs. the content c(Bm) of boehmite in products formed in HTT of gibbsite at 200–210°C (pH 10.5).

The dissolution–precipitation mechanism accounts for the close sizes of primary gibbsite and boehmite particles in the initial period of HTT, when the fraction of the phase being formed is still small and for the incoherent increase in the CSR size of boehmite crystals by no more than 22–24 nm at a boehmite content of a sample close to 100 wt % (Fig. 1). Boehmite crystallizes on the surface of thin gibbsite plates formed as a result of the dehydration and intense delamination of its crystals along the (001) plane and the subsequent hydroxylation of this plane, as indicated by an analysis of IR spectra of the samples in the range of stretching vibrations of interlayer [ν(OH)] = 3528 cm^{-1}] and terminal [ν(OH) = 3624 cm^{-1}] hydroxy groups situated on the (001) plane (Table 4). The intensity ratio of the above absorption bands in the IR spectrum of the starting gibbsite, I_{3528}/I_{3624} = 1.82. After the HTT, the I_{3528}/I_{3624} ratio decreases to 1.30 for the sample containing only 5 wt % boehmite (Fig. 2), whose IR spectrum contains very weak absorption bands associated with stretching vibrations of the structural hydroxy groups [ν_s(OH) = 3292 cm^{-1} and ν_{as}(OH) = 3093 cm^{-1}] corresponding to the monohydroxide being formed. Consequently, after gibbsite crystals undergo delamination and the number of interlayer OH groups in its structure decreases, the number of terminal OH groups on the (001) plane increases, with this occurring to an extent exceeding that theoretically possible at a proportional amount of transformed gibbsite.

This increase in the fraction of the terminal OH groups relative to that of the interlayer groups may be due both to the enhanced hydroxylation of the (001) plane in the

Table 3. Effect of the gibbsite HTT conditions on the ^{27}Al chemical shift and the concentration of aluminum atoms in the mother liquor according to ^{27}Al NMR data

HTT conditions			δ, ppm	*c*(Al), mM
T, °C	τ, min	pH		
200	30	10.5	80.7	0.08
	60			0.43
	60	8.0		0.11
	60	6.0		0.01
210	30	10.5		0.75
	60			1.06

Table 4. Effect of the concentration of unconverted gibbsite on the intensity ratio of the absorption ands in the IR spectra of HTT products

c(Gb), wt %	I_{3528}/I_{3624}
95.0	1.30
78.0	1.50
71.0	1.40
52.1	1.48
49.1	1.52
45.4	1.30
14.1	1.41

Table 5. Parameters of the mesoporous system of products formed in HTT orthoferrite according to the low-temperature nitrogen adsorption data

HTT conditions			*c*(Bm), wt %	S_{BET}, $m^2\ g^{-1}$	D_{max}, nm	dV/dD, $cm^3\ g^{-1}\ nm^{-1}$
T, °C	*t*, min	pH				
Starting gibbsite			–	0.1	3.7 7.0 ~10.0–50.0	0.6 0.2 0.1
180	180	10.5	22.0	0.5	2.3 ~10.0–50.0	21.9 2.3
	90		42.5	1.0	2.2 ~10.0–50.0	6.6 4.5
190	120	10.5	68.4	0.5	4.1 ~20.0–300.0	15.3 2.2
	150		91.1	0.4	4.1 ~20.0–300.0	29.9 1.7
	180		100.0	1.3	2.6 3.9 ~20.0–300.0	87.7 53.8 5.7
190	180	8.0	100.0	0.8	1.7 3.9 ~20.0–300.0	86.0 28.2 3.5
190	120	6.0	47.9	1.0	2.3 ~10.0–50.0	152.4 10.8
	180		98.7	0.9	2.3 4.1 ~20.0–300.0	39.0 36.4 2.1
200	90	10.5	100.0	1.3	2.3 3.9 ~20.0–300.0	28.2 81.2 3.0
	105		100.0	0.7	4.1 ~20.0–300.0	59.5 3.7
	120		100.0	1.2	2.3 3.9 ~20.0–200.0	44.0 134.0 4.0

Table 6. Effect of the HTT conditions on the floccule diameter distribution and on the abrasion resistance of floccules

HTT conditions			D_{max}^{fl}, μm	Floccule distribution, wt %, in indicated diameter ranges, μm				RA, %
T, °C	τ, min	pH		< 1	1–20	20–100	> 100	
Starting gibbsite			80.1	–	–	80.9	19.1	92.0
180	180	10.5	80.0	–	–	81.0	19.0	60.6
190	180	10.5	80.0	–	–	80.0	20.0	0
200	180	10.5	14.0 0.6 0.2	22.7	73.0	4.3	–	0

aqueous medium and to the increase in the number of such planes, which is probably favored by the accelerated dehydration of gibbsite. For example, the intensity ratio I_{3528}/I_{3624} of the absorption bands in the IR spectra of HTT products with boehmite concentrations of 5 to 86 wt %, varies within the narrow range from 1.3 to 1.5. Thus, just in the HTT on a multitude of (001) planes there occurs nucleation and growth of boehmite crystals by the dissolution–precipitation mechanism. Extended layers of gibbsite crystals stand out in the cross-sectional SEM images of floccules of a sample produced by HTT at 180°C for 180 min [*c*(Bm) = 22.0 wt %]. These parallel layers have thicknesses of 20–100 nm, with rare cracks with widths of 10–50 nm formed in between. It can be seen that the dissolution of gibbsite crystals is manifested in a pronounced erosion of outer layers of the crystals, and boehmite nuclei are deposited directly on the (001) planes of gibbsite. The faces of the primary boehmite particles are arranged in parallel to the precursor faces. Further growth of crystals is also possible out of a gibbsite crystal.

The phase transitions in the HTT of gibbsite lead to insignificant changes in the mesoporous system of the samples. As shown previously [20], gibbsite is a nonporous compound because of the close packing of its primary crystals and secondary particles. A more detailed analysis of the mesoporous system demonstrated that S_{BET} of gibbsite does not exceed 0.1 $m^2 g^{-1}$ (Table 5). In the differential curves of pore volume distributions, mesopores are manifested as narrow peaks at diameters of 3.7 and 7.0 nm and by a wide peak at diameters of 10.0–50.0 nm (Fig. 6a). All these pores have the form of slits because the adsorption isotherm belongs to type II with an H3 hysteresis loop (Fig. 6b) and, according to SEM data, separate cracks in coarse aggregates orthoferrite crystals (Fig. 3).

Comparison of the SEM results and data in Table 5 shows that the delamination of gibbsite crystals and the simultaneous formation of boehmite crystals in an amount of up to 50 wt % is accompanied by a slight increase in the specific surface area to 0.5–1.0 $m^2 g^{-1}$ due to the appearance of new slit-like mesopores (Fig. 6b) with a diameter of 2.2–2.3 nm and additional mesopores with diameters of 10.0–50.0 nm. The formation of these latter is indicated by a more than 130-fold increase (from 0.1×10^{-5} to 10.8×10^{-5} $cm^3 g^{-1} nm^{-1}$) in the intensity of the peak at diameters of 10.0–50.0 nm in the differential curve of pore volume distributions (Table 5). Comparison of the SEM data and results of a low-temperature adsorption of nitrogen makes it possible to attribute the pores with diameters of 10.0–50.0 nm to slits between the (001) planes in gibbsite crystals. In turn, the possible origin of the pores with diameters of 2.2–2.3 nm are spaces between close-packed primary crystals of boehmite being formed.

As the concentration of boehmite in the samples reaches values of 70–100 wt %, the specific surface area grows to only 1.3 $m^2 g^{-1}$. The changes in the specific surface area are insignificant because the crystallization of boehmite and growth of its particles are accompanied by broadening of the pores considered above to diameters of 3.9–4.1 and 20.0–300.0 nm (Table 5). The appearance of the coarse mesopores is due to the coarsening of boehmite particles to 4 μm and loosening of the internal structure of floccules because of the chaotic packing of these particles (Fig. 3).

The disordered distribution of coarse boehmite particles within the floccules to a substantial decrease in their abrasion resistance (RA) from 92% for the starting gibbsite to 60.6% upon the formation of 22.0 wt %

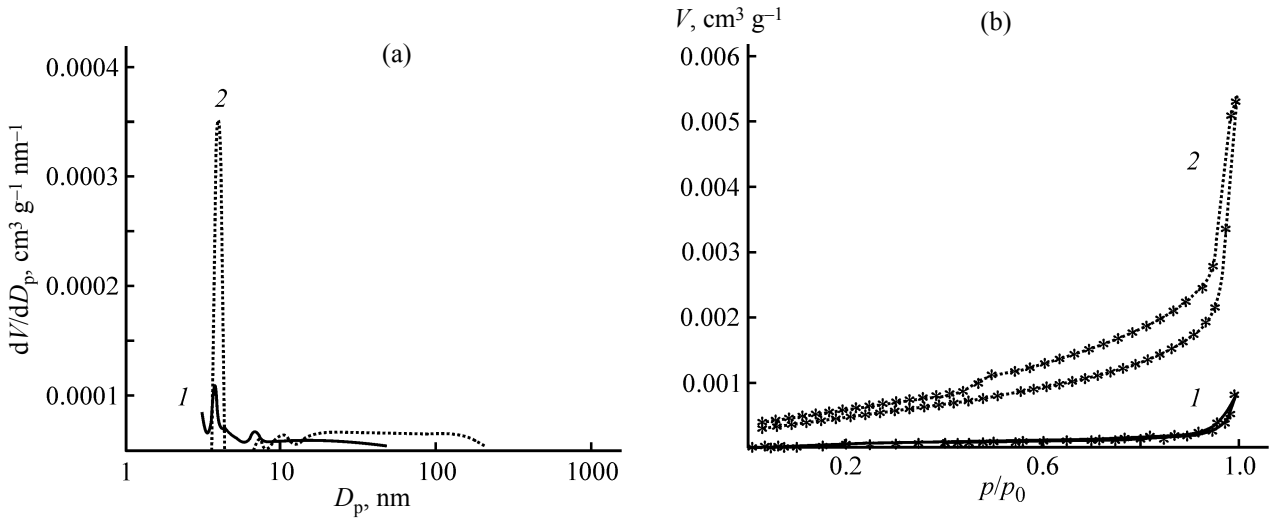

Fig. 6. (a) Differential curves of the volume V distribution over pore diameters D_p and (b) nitrogen adsorption–desorption isotherms. (p/p_0) Relative pressure. (*1*) Starting gibbsite and (*2*) HTT product obtained at T = 190°C, τ = 90 min, and pH 10.5.

boehmite (T = 180°C, τ = 180 min, pH 10.5), and down to zero upon the complete recrystallization into boehmite (Table 6).

We attribute the so significant decrease in the floccule strength to the specific feature of the phase transition of gibbsite into boehmite by the dissolution–precipitation mechanism, with the crystallization bonds between particles of the preceding phase, which form the floccule skeleton, disintegrated. As the size of boehmite nuclei precipitated on planes of gibbsite crystals increases to 4 μm, the nuclei form no stable crystallization bonds with each other. In the process, the floccules may preserve the original form of the precursor, as in the case of samples obtained in HTT at 180 and 190°C, whose particle size distribution is identical to that in the starting gibbsite and is characterized by the only strong peak at a diameter D^{fl}_{max} of 80 μm (Table 6). Despite this circumstance, the poor abrasion resistance of floccules and the small specific surface area give no way of their application as catalyst supports. On raising the temperature to 200°C, floccules are strongly dispersed to particle sizes less than 20 μm, with the share of these reaching a value of 96% (Table 6).

CONCLUSIONS

(1) Gibbsite floccules are aggregates of two kinds of primary particles, of which about 30 wt % have average coherent scattering region sizes of up to 76.1 nm along the (002) plane and up to 74.9 nm along the (110) plane, and 70 wt %, up to 106.2 nm along the (002) plane and up to 88.8 nm along the (110) plane.

(2) Under the hydrothermal conditions in an aqueous suspension at pH 6.0–10.5, the complete phase transition of gibbsite into boehmite occurs in 180 min at 190°C, 120 min at 200°C, and 20 min at 210°C. The apparent activation energy of the process is 172 ± 7 kJ mol^{-1}.

(3) As a result of the hydrothermal treatment, primary boehmite particles are formed as rhombs or parallelepipeds with coherent scattering region sizes of 60.5 to 82.7 nm along the (020) plane and 35.9 to 59.6 nm along the (120) plane. At a low temperature (T = 180°C) and long hydrothermal treatment (150–240 min) or at high temperature (T = 190–200°C) and short time (20–90 min) of hydrothermal treatment and comparatively low water vapor pressures (1.0–1.6 MPa), smaller primary gibbsite particles undergo a phase transition, whereas at high (1.9 MPa) water vapor pressures, there occurs recrystallization of coarser primary gibbsite particles.

(4) The phase transition of gibbsite into boehmite occurs under hydrothermal transitions in an aqueous suspension by the dissolution–precipitation mechanism after a strong delamination of gibbsite crystals along the (001) plane to give a multitude of layers with thicknesses of 20–100 nm and cracks with widths of 10–50 nm in between. The dissolution of gibbsite is accompanied by release into the mother liquor of $[Al(OH)_4]^-$ anions interacting with protons of hydroxy groups on (001) planes with the subsequent formation of boehmite nuclei and growth of their crystals.

(5) The close packing of primary particles of the crystallizing boehmite is responsible for the formation of nonporous floccules with S_{BET} = 0.7–1.3 $m^2 g^{-1}$.

(6) The disordered distribution within the floccules of coarse boehmite particles forming no crystallization bonds with each other is responsible for the decrease in their abrasion resistance, which decreases to zero upon the complete phase transition of gibbsite into boehmite. This circumstance gives no way of using the method of a direct phase transition of gibbsite into boehmite under hydrothermal conditions in an aqueous suspension to obtain microspherical aluminum oxide catalyst supports.

ACKNOWLEDGMENTS

The study was supported by the Ministry of Education and Science of the Russian Federation.

REFERENCES

1. Flid, M.R. and Treger, Yu.A., *Vinilkhlorid: khimiya i tekhnologiya V dvukh knigakh* (Vinyl Chloride: Chemistry and Technology n two books), Moscow: Kalvis, 2008, book 1.
2. Mukhlenov, I.P. and Pomerantsev, V.M., *Kataliz v kipyashchem sloe* (Catalysis in Fluidized Bed), Leningrad: Khimiya, 1978.
3. Egorova, S.R. and Lamberov, A.A., *Russ. J. General Chem*., 2014, vol. 84, no. 12, pp. 1942–1953.
4. Lopushan, V.I., Kuznetsov, G.F., Pletnev, R.N., et al., *Izv. Ros. Akad. Nauk, Ser. Fiz*., 2007, vol. 71, no. 8, pp. 1222–1224.
5. Egorova, S.R., Lamberov, A.A., Kataev, A.N., et al., *Katal. Prom–sti*, 2008, no. 6, pp. 47–54.
6. Inoue, M., Tanino, H., Kondo, Y., et al., *Clays Clay Miner*., 1991, vol. 39, no. 2, pp. 151–157.
7. Panasyuk, G.P., Belan, V.N., Voroshilov, I.L., et al., *Neorg. Mater*., 2010, vol. 46, no. 7, pp. 831–837.
8. Ivankin, Yu.D., Zui, A.I., Murav'eva, G.P., et al., *Vestn. Mosk. Univ., Ser. 2 Khim*., 2001, vol. 42, no. 4, pp. 258–262.
9. Tolchev, A.V., Lopushan, V.I., and Kleshchev, D.G., *Neorg. Mater*., 2011, vol. 37, no. 12, pp. 1493–1496.
10. Kuznetsov, V.A., *Kristallografiya,* 1967, vol. 12, no. 3, pp. 702–707.
11. Oh, Ch.J., Yi, Y.K., Kim, S.J., et al., *Powder Technol*., 2013, vol. 235, pp. 556–562.
12. Madarasz, J., Pocol, G., Novak, C., et al., *J. Therm. Anal*., 1992, vol. 38, pp. 445–454.
13. Panda, P.K., Jaleel, V.A., and Devi, S.U., *J. Mater. Sci*., 2006, vol. 41, pp. 8386–8389.
14. Tsuchida, T., *J. Eur. Ceram. Soc*., 2000, vol. 20, pp. 1759–1764.
15. Novak, C., Pokol, G., Izvekov, V., et al., *J. Therm. Anal*., 1990, vol. 36, no. 10, pp. 1895–1909.
16. Gregg, S.J. and Sing, K.S.W., *Adsorption Surface Area and Porosity*, London: Academic Press, 1967.
17. Brown, M., *Reactions in the Solid State*, Elsevier Science, 1980.
18. Matheu, Y., Rigolet, S., Valtev, V., et al., *J. Phys. Chem*., 2008, vol. 112, pp. 18384–18392.
19. Panias, D., Asimidis, P., and Paspaliaris, I., *Hydrometallurgy*, 2001, vol. 59, pp. 15–29.
20. Egorova, S.R. and Lamberov, A.A., *Russ. J. Appl. Chem*., 2014, vol. 87, no. 8, pp. 1021–1030.